

Monte Carlo study of dose distribution improvement by skin-shielding layer design in boron neutron capture therapy for non-small-cell lung cancer

X. Tang^{1,2,*}, H. Yu¹, D. Shu¹, C. Gong¹, C. Geng^{1,2}, Y. Ai¹ and D. Chen^{1,2}

¹ Department of Nuclear Science and Engineering, Nanjing University of Aeronautics and Astronautics, Nanjing 210016, P.R. China.

² Collaborative Innovation Center of Radiation Medicine of Jiangsu Higher Education Institutions, Nanjing 210016, P.R. China.

Received: 19 April 2017 / Accepted: 25 May 2018

Abstract – The skin dose exceeds its dose limitation easily in using an accelerator-based neutron source for non-small-cell lung cancer (NSCLC) with boron neutron capture therapy (BNCT). To solve this problem, design analyses in materials and thicknesses of skin-shielding schemes were investigated through Monte Carlo method. Two skin-shielding schemes were better and could reduce the healthy organ dose: scheme A (0.1 cm-thick thermoplastic with 96%-enriched ⁶LiF), and scheme B (0.6 cm-thick lithium carbonate). Scheme B with shorter irradiation time was the optimized schemes to improve the dose distribution of BNCT for NSCLC.

Keywords: BNCT / non-small-cell lung cancer / skin dose / dose assessment / Monte Carlo method

1 Introduction

Local non-small-cell lung cancer (NSCLC) is a common tumor, with its tumor locations mostly near the trachea and which have diffused into the lungs but not into the whole body, and it requires timely treatment. Boron neutron capture therapy (BNCT), which combines the advantages of molecular targeting and heavy ion therapy, is considered an alternative therapeutic approach for the limb osteosarcoma attributed to its high Linear Energy Transfer (LET) and higher Relative Biological Effectiveness (RBE), for the reaction ¹⁰B(n, alpha)⁷Li generates an alpha particle and a ⁷Li nucleus with ranges comparable to cell diameters (Fujimoto *et al.*, 2015). Scholars have proposed BNCT of NSCLC (Kiger, 2006), for this therapy can avoid the inaccurate treatment caused by the motions of cancerous lung tissues during photon radiotherapy, as the major dose deposition of BNCT depends on boron localization. Moreover, the treatment may be delivered in a single-fraction through BNCT with less time.

Clinical studies on BNCT indicate that the neutron source and distribution of boron concentration are key factors affecting the curative effect of this therapy (Sutlief, 2015). The energy spectrum of the neutron sources and the boron distribution in human play important roles in the dose deposition (Sakurai and Ono, 2007) in cancer patients. Dose delivery to healthy organs increases with increasing boron

concentration in healthy tissues, and this phenomenon leads to increased cancer risk (Ryynanen and Kortensniemi, 2000). Thus, adjustable neutron source and boron drug with high concentration in cancer cell need to be continuously developed. At present, the study of BNCT for NSCLC mainly includes clinical experiments (Trivillin *et al.*, 2004; Bortolussi *et al.*, 2011) and theoretical research (Farias *et al.*, 2014; Krstic *et al.*, 2014) in different country. In 2012, Suzuki studied the re-irradiation for lung cancer in clinic with BNCT in Japan (Suzuki *et al.*, 2012). However, the treatment effect was not very good for unsatisfactory dose distribution. Since 2014, we have been studying the BNCT of NSCLC with Monte Carlo method, which aims to provide references for the clinic treatment of BNCT of NSCLC. We have explored the impacts of boron concentration and neutron source on different types of tumors (Haiyan *et al.*, 2017a) and multi-field neutron source irradiation during the BNCT of NSCLC (Haiyan *et al.*, 2017b).

Until now, nuclear reactors are used commonly in BNCT treatment, and accelerator-based neutron source used for treatment has not been reported yet. Indeed, due to the advantage of compact with less cost, the accelerator-based neutron source have a trend to be widely used in hospital. However, in the case of accelerator-based neutron source irradiation, as the lung cancer reaches the prescription doses, the skin dose often exceeds its dose limitation (Krstic *et al.*, 2014). In conventional radiotherapy of electron and photon beams, some researchers have put forward a protective layer on the skin surface to decrease skin dose (Norbash *et al.*, 1996; Liu *et al.*, 2013). Nevertheless, for BNCT of NSCLC, an

*Corresponding author: tanxiaobin@nuaa.edu.cn

Table 1. BNCT in-air parameters of IAEA recommended and Neuboron source.

Configuration	ϕ_{epi} ($\times 10^9 \text{ cm}^{-2} \text{ s}^{-1}$)	ϕ_{th} / ϕ_{epi}	D_f / ϕ_{epi} ($\times 10^{-13} \text{ Gy cm}^2$)	D_γ / ϕ_{epi} ($\times 10^{-13} \text{ Gy cm}^2$)
IAEA Limits	≥ 1	~ 0.05	≤ 2	≤ 2
Neuboron source	1.3	0.04	2.05	1.24

The epi/th represent the flux ratio of epithermal neutron to the thermal neutron.

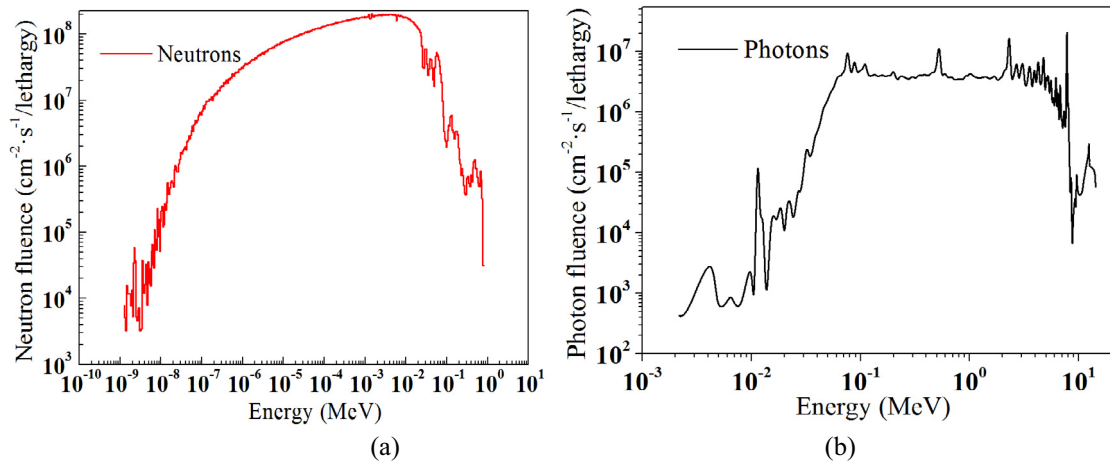


Fig. 1. (a) Neutron and (b) photon fluence rate per unit of lethargy as a function of energy for the Neuboron source (Lee *et al.*, 2014).

in-depth study on the reduction of skin dose has not been conducted. Thus, to improve the dose distribution and feasibility of BNCT for NSCLC, various skin-shielding schemes were designed. The general-purpose Monte Carlo particle transport code MCNP5 was employed to simulate the dose calculations in this study. Through the comparisons of the irradiation time and dose distribution of different schemes, an ideal design scheme was chosen to improve the dose distribution in BNCT.

2 Materials and methods

2.1 Neutron source

A neutron beam called “Neuboron neutron source” is under construction by Neuboron Medtech Ltd. (Neuboron, China), and the proton accelerator is provided by Budker Institute of Nuclear Physics (BINP, Russia) (Bayanov *et al.*, 2015). The accelerated based neutron is produced from the reactions of protons and lithium target ${}^7\text{Li}$ (p, n) ${}^7\text{Be}$. After the beam shaping assembly designed by Lee and Liu (Lee *et al.*, 2014), the characteristics of the Neuboron source are in accordance with the criteria recommended by the International Atomic Energy Agency (IAEA) (IAEA, 2001) as shown in Table 1, and its neutron and photon energy spectra are shown in Figure 1.

The Neuboron source was set as a disc non-point source. The diameter of the source was 20 cm. It could completely encompass the tumor volume. The larger the source skin distance (SSD) is, the larger the radiation field will be. Thus, in

order to reduce the dose to healthy tissue as far as possible, the SSD was chosen to be 3 cm. In addition, the angular distribution of the neutron emitted from source/BSA is approximate considered as cosine law distribution (cosine=0.67) in the MCNP input configuration, for the real angular distribution is complicated and is difficult to acquire. The epithermal neutron fluence of the beam was $1.3 \times 10^9 \text{ cm}^{-2} \cdot \text{s}^{-1}$.

2.2 CHRP-M30 Phantom implementation

A dose calculation model was established based on a 30-year-old male of Chinese hybrid radiation phantom (CHRP-Male 30) (Geng *et al.*, 2014) (Fig. 2). The high-precision male phantom was built in Rhinoceros 5.0 (Guitton *et al.*, 2013), and voxelizer series tools were employed to transform the phantom into a voxel-based model. In considering the precision of the geometry construction and the calculation speed in the Monte Carlo calculation, the phantom was voxelized with a resolution of $0.4 \times 0.4 \times 0.4 \text{ cm}^3$. Tissue and organ compositions were taken from the data in ICRU-46 (ICRU 46, 1992) and ICRP-89 (ICRP 89, 2002). Details of the construction procedure for the phantom geometry and materials have been described in a previous publication (Geng *et al.*, 2014). Based on the CHRP-Male 30 phantom, the tumor (depth of 7 cm) was established (Fig. 2) according to the common NSCLC. The gross tumor volume (GTV) was approximately $7 \times 4 \times 3 \text{ cm}^3$, and the cancerous lung was divided into healthy lungs (black) and the GTV (purple). This tumor-prescribed dose was set as 32 Gy-Eq (Farias *et al.*, 2014).

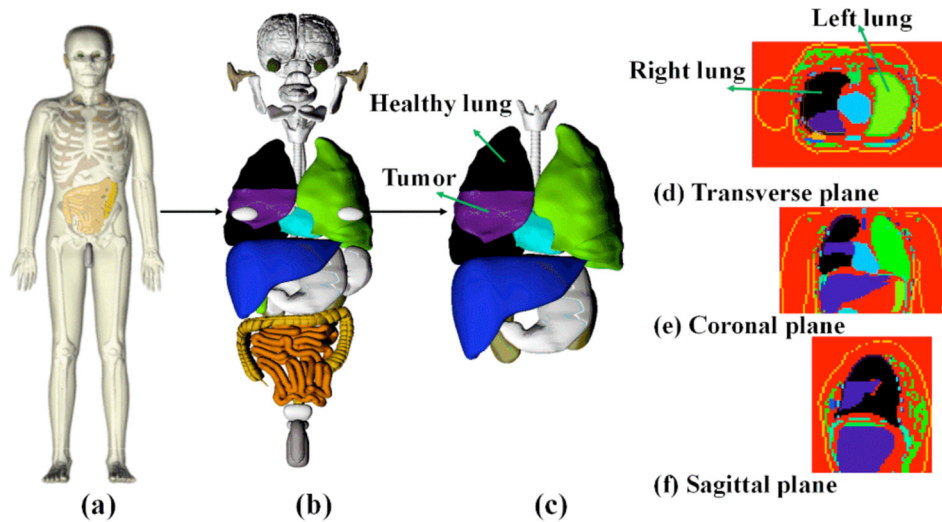


Fig. 2. Implementation and three views of the NSCLC model defined in the CHRP-Male 30 phantom.

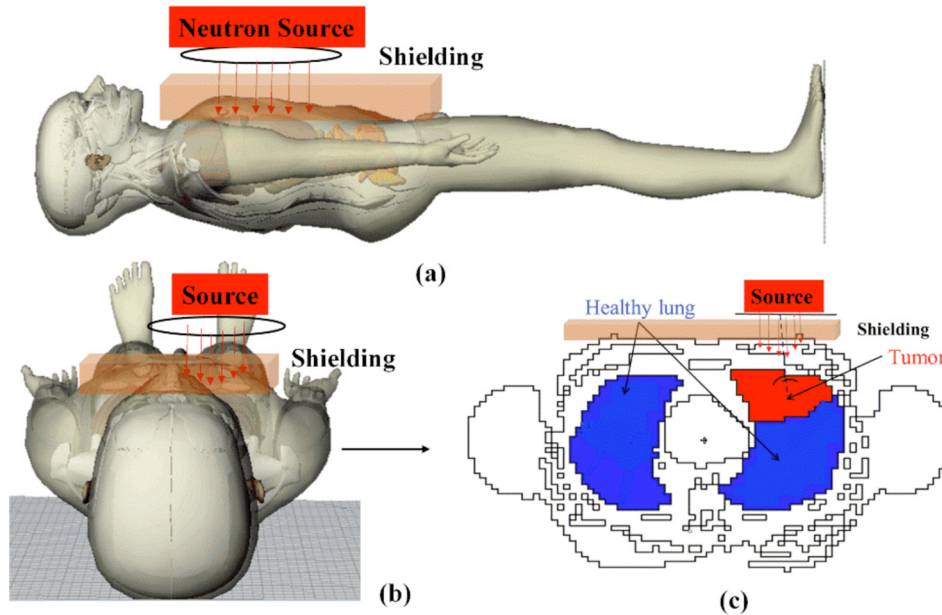


Fig. 3. Neutron irradiation planning and skin shielding design: (a) lateral view; (b) vertical view; and (c) cross section of lung cancer irradiation. In this case, healthy lungs (blue) and the tumor area GTV (red) were marked.

The ^{10}B concentrations in tumor and in skin were assumed as 48 ppm and 9 ppm, which could guarantee that treatment time is around 30 min. The ratio of ^{10}B concentration in the skin to that in other healthy tissues was 1.5:1. In this case, the ^{10}B concentration was considered as a constant.

2.3 Skin-shielding layer design

Skin-shielding layer design was proposed to reduce the skin dose and improve the dose distribution (Lee *et al.*, 2014). The skin-shielding layer was added between the neutron source and the skin surface. The skin-shielding layer covered the whole chest of phantom, and their length-width of skin shield was 100 cm \times 80 cm. The thicknesses were 0.1, 0.2, 0.3,

0.4, 0.5, 0.6, 0.8 and 1 cm, which represented the distance between the skin surface and the upper surface of shielding material on the center shaft of the neutron beam. Three kinds of layer materials were considered in this work, *i.e.* Equivalent Tissue material (ETM), thermoplastic with 96%-enriched ^6LiF ($^6\text{LiF-TP}$, the quality ratio of ^6LiF to thermoplastic is 4:6) (Sakurai and Ono, 2007), and lithium carbonate (Li_2CO_3 , the quality ratio of $^6\text{Li}_2\text{CO}_3$ to $^7\text{Li}_2\text{CO}_3$ is 1:3). The three materials were placed on the surface of the chest (Fig. 3).

2.4 Dose calculations and treatment assessments

The dose of BNCT includes boron dose (D_B), thermal neutron dose (D_{th}), fast neutron dose (D_f), and gamma dose

Table 2. RBE and CBE factors used to convert the absorbed dose (Gy) into biological dose (Gy-Eq) (Ishiyama, 2014).

BNCT dose component	Normal tissues	Tumor	Skin
$^{10}\text{B}(n,\alpha)^7\text{Li}$ (CBE)	1.4	3.8	2.5
Thermal neutron (RBE)	3.2	3.2	3.2
Fast neutron (RBE)	3.2	3.2	3.2
Photon	1	1	1

(D_γ). The boron dose stems from the interaction of thermal neutrons with ^{10}B atoms in the tissue and goes through the $^{10}\text{B}(n,\alpha)^7\text{Li}$ reaction. The thermal neutron dose arises primarily from the thermal neutron capture reaction of $^{14}\text{N}(n,p)^{14}\text{C}$. The fast neutron dose comes from fast neutrons with energies above 10 keV delivering the dose through elastic collisions with hydrogen nuclei in the tissue. The gamma dose is generated from an unavoidable gamma contamination of the beam and the induced gamma dose in the tissues.

Biological dose of BNCT was computed by multiplying each absorbed dose component by the relative biological effectiveness (RBE) or the compound biological effectiveness (CBE) factors listed in Table 2. It was calculated as follows:

$$HT = \omega_B \times D_B + \omega_{th} \times D_{th} + \omega_f \times D_f + D_\gamma. \quad (1)$$

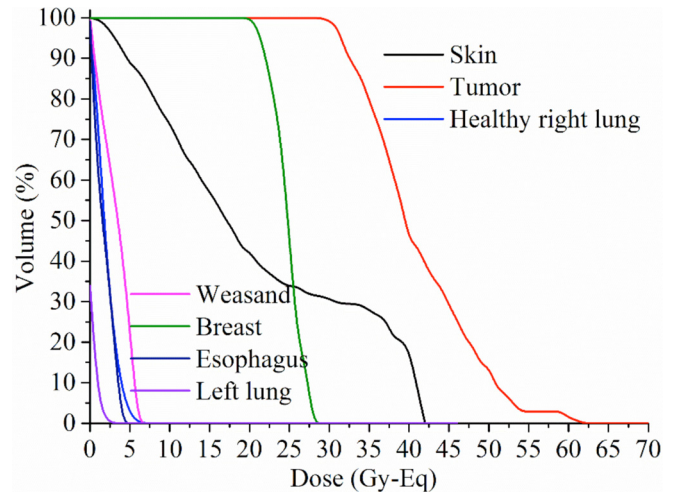
Different skin-shielding schemes were evaluated through dose to organs at risk (OARs). The doses to OARs (including skin, right healthy lung, esophagus, heart, liver, breast, and trachea) were selected to characterize dose distribution and estimate the efficacy of BNCT treatment, according to their average dose, maximum dose, and treatment time. In addition, in comparing the dose distribution of tumor or OARs, the dose volume curves (DVCs) and second cancer risks of the OARs were depicted.

The dose to OARs should meet two limitations, according to the National Comprehensive Cancer Network (NCCN) (Ettinger *et al.*, 2013), as follows. First, more than 1000 cm^3 of the volume of the healthy lung should receive less than 7.5 Gy-Eq to prevent pneumonia. Second, the maximum dose to the heart, spinal cord, skin, esophagus, trachea, ribs, and breast should be less than 22, 14, 26, 15.4, 20.2, 30 and 30 Gy-Eq, respectively.

2.5 Monte Carlo configurations

The MCNP5 version of MCNP5_RSICC, 1.14 was used to perform the dose calculations in this study. The universe/lattice card was employed in constructing the human voxel phantom. The SDEF card defined the disc non-point sources for Neutron, and different concentrations of ^{10}B were added in Material Cards of tumor and OARs. The MT card was used to fix the thermal reaction cross section.

The doses to the tumor and OAR were calculated through the tally F4 combined DE/DF cards. For the dose conversion, pointwise kerma factors and energy mass absorption coefficients from the reference (Goorley *et al.*, 2002) were input

**Fig. 4.** Dose distribution in tumor and OARs.**Table 3.** Maximum dose to OARs and their dose limitation of NCCN guidelines.

Organs at risk	Maximum dose (Gy-Eq)	Limited dose (Gy-Eq)	Difference (%)
Breast	26.00	30.00	-13.30
Heart	17.50	22.00	-20.40
Esophagus	4.50	15.40	-68.80
Tracheal	7.00	20.20	-62.80
Skin	42.00	26.00	+61.50
Rib	17.30	30.00	-42.30
Spinal cord	3.40	14.00	-75.70

with DE and DF cards directly. To obtain the neutron spectrum, tally F4 was used to estimate the neutron fluence.

The parallel calculation with 64 cores in one computer is used to calculate the dose. The number of simulated source particles was set as 1×10^9 in all simulations to keep the statistical uncertainty below 2% for the dose results in all the organs of interest.

3 Results

3.1 Tumor and OAR dose without skin-shielding layer

The doses to OARs were calculated without a skin-shielding layer. The tumor dose reached a prescribed dose of 32 Gy-Eq (Farias *et al.*, 2014) (Fig. 4) after 26.1 min irradiation, and the maximum doses to chest organs or tissues were within their limits (Tab. 3). The maximum doses to the left and right lung were 3 Gy-Eq and 6 Gy-Eq, respectively, which fully conformed to the NCCN guideline (Ettinger *et al.*, 2013).

However, the skin dose obviously exceeded its dose limit. The maximum dose to the skin was 42 Gy-Eq, and 30% of the volume of the skin received more than its dose

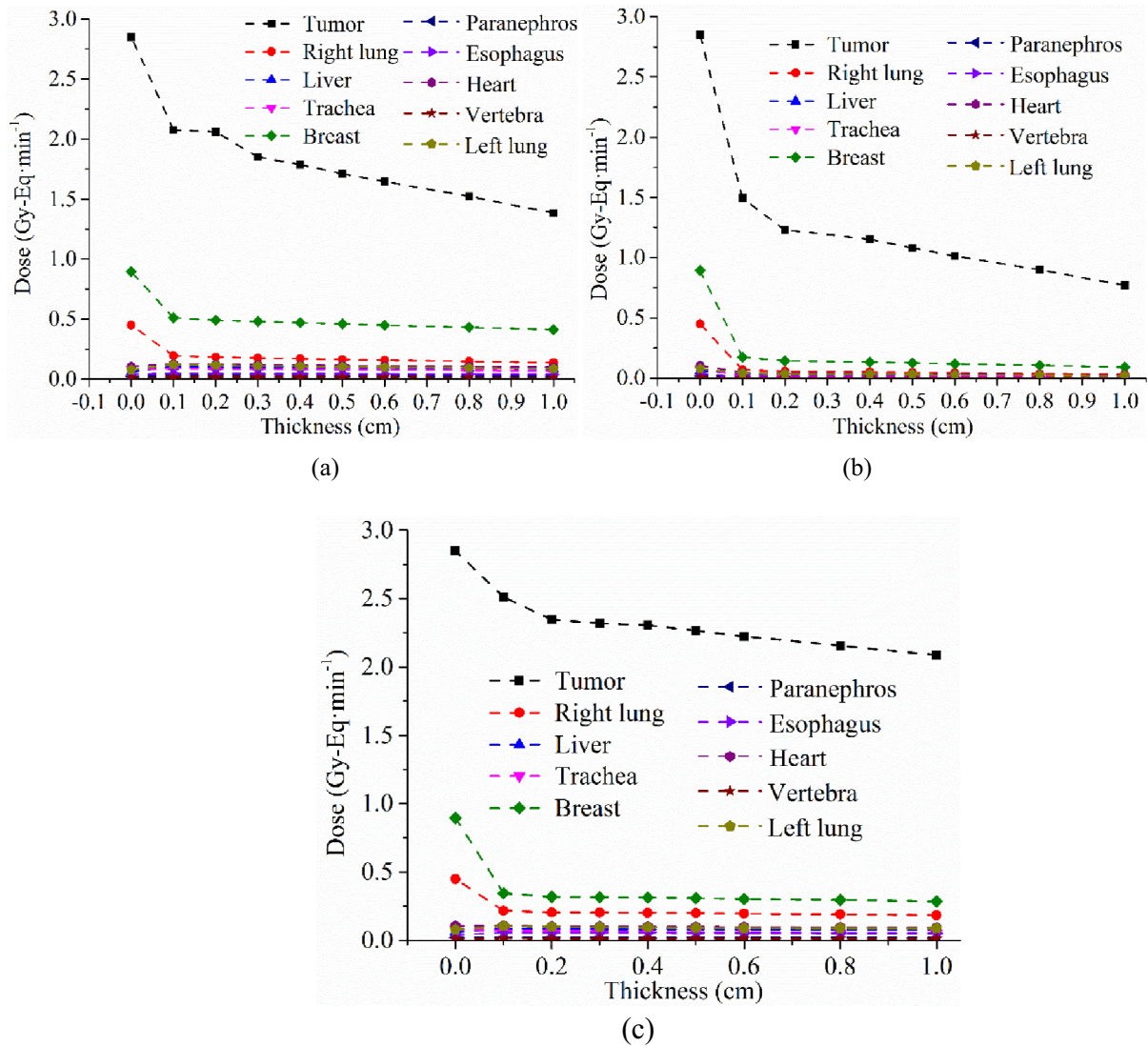


Fig. 5. Average dose rates to tumor and healthy organs with three materials used as the skin-shielding layer: (a) ETM, (b) ⁶LiF-TP, and (c) lithium carbonate (Li₂CO₃).

limit of 26 Gy-Eq (Ettinger *et al.*, 2013) (Fig. 4). Thus, the skin dose must be reduced by adding a skin-shielding layer in treatment.

3.2 Influence of skin-shielding layer on dose and neutron flux

When ETM was used as a skin-shielding layer, the healthy tissue dose rate was reduced slightly, but the tumor dose exhibited a large attenuation (Fig. 5a). When ⁶LiF was used, tumor average dose rates decreased obviously (Fig. 5b). In addition, when Li₂CO₃ was used, the average dose rate to the tumor was higher than that when ⁶LiF was used, and the OAR dose was slightly affected by Li₂CO₃ (Fig. 5c). In the actual treatment, doses to tumor and skin and treatment time need further consideration to choose the optimal scheme.

Moreover, the neutron spectra after passing through different thicknesses of shields were calculated in Figure 6. The neutron fluxes after the shields of ETM, ⁶LiF-TP and Li₂CO₃ were presented in Figure 6a, b and c. Their epithermal neutron fluxes were also calculated, which were presented in Figure 6d. With the skin shields added, the fast neutron flux decreased, and the thermal neutron increased. As the shields became thicker, the changes were more evident. Especially in the ETM, when ETM shield reached 1 cm-thick, the thermal neutron flux reached $2.5 \times 10^8 \text{ cm}^{-2} \cdot \text{s}^{-1}$. In addition, with the increasing thickness of all shields, the epithermal neutron fluxes all have the trend to get its maximum, and then turned down (Fig. 6d). The reason is that fast neutrons were converted to more epithermal neutrons with the moderation of thin shields; as shields became thicker, the attenuations of epithermal neutrons were more obvious than the increase of epithermal neutrons.

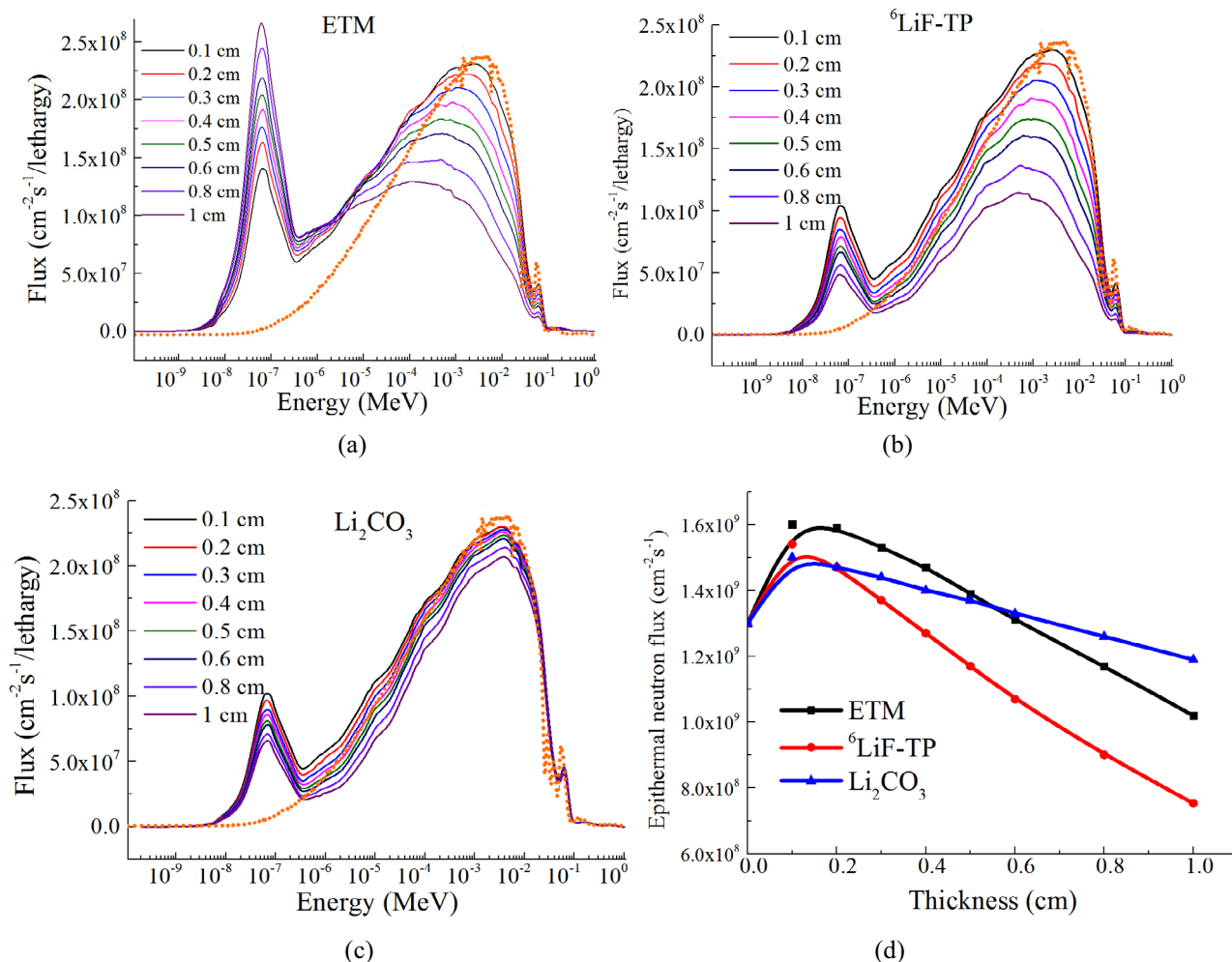


Fig 6. The neutron flux after passing through different shields of (a) ETM, (b) ⁶LiF-TP, (c) Li₂CO₃, and (d) is their epithermal neutron fluxes at different thicknesses.

Furthermore, the influence of the thickness of different materials on the treatment time and skin dose was studied, when the tumor reached the prescription dose of 32 Gy-Eq. The following factors were considered:

- the skin dose must be within its dose limitation of 26 Gy-Eq;
- the irradiation time should be within the appropriate range, preferably half an hour or less;
- the thickness should be as small as possible.

As shown in Table 4, when ETM was used as a skin-shielding layer, the maximum dose to the skin exceeded the dose limit of 26 Gy. Thus, ETM was not suitable as a skin-shielding layer. For ⁶LiF-TP and lithium carbonate, the two best schemes were selected. Scheme A involved 0.1 cm-thick ⁶LiF-TP, and scheme B involved 0.6 cm-thick lithium carbonate.

In addition, the epithermal neutron fluxes of scheme A (0.1 cm ⁶LiF-TP) and scheme B (0.6 cm Li₂CO₃) both meet the recommended in-air criteria of $1.0 \times 10^9 \text{ cm}^{-2}\cdot\text{s}^{-1}$, and their other IAEA recommended in-air criteria also approached the recommended value (Tab. 5).

3.3 Influence of shielding schemes on dose composition

In studying the physical mechanism for skin dose reduction under the conditions of scheme A and scheme B, the dose compositions in the tumor and healthy organs (especially skin) were compared under the two shielding schemes. For the condition without a skin-shielding layer, the tumor and OAR dose components are shown in Figure 7a. The dose in this condition was considered as the original dose.

The dose rate to the tumor and healthy organs decreased obviously in the condition of shielding by scheme A. For the tumor dose, the average dose rate reduced to 52.5% of the original; its fast neutron dose decreased, and the proportion of the boron dose increased. For the skin dose, the average dose rate reduced to 17.0% of the original (Fig. 7b). All dose components of the skin decreased. In particular, the fast neutron dose reduced to 10% of the original value.

Under shielding by scheme B, the reduction of tumor dose was less than that by scheme A. In addition, its boron dose and thermal neutron dose decreased. The average dose to the skin

Table 4. Treatment time and maximum dose to skin with different thicknesses of the three materials.

Thickness (cm)	Materials					
	Equivalent Tissue material		⁶ LiF-TP		Lithium carbonate	
	Treatment time (min)	Skin maximum dose (Gy-Eq)	Treatment time (min)	Skin maximum dose (Gy-Eq)	Treatment time (min)	Skin maximum dose (Gy-Eq)
0.1	28.88	34.08	40.05	20.82	26.89	28.06
0.2	32.40	38.08	48.86	23.42	28.56	29.65
0.3	32.90	34.03	50.84	22.37	28.86	29.71
0.4	34.52	33.12	52.11	19.28	29.01	26.80
0.5	35.04	33.52	55.62	18.02	29.48	24.54
0.6	36.40	34.72	59.30	17.61	29.97	23.57
0.8	39.36	36.64	66.81	17.50	31.52	23.72
1	43.28	39.20	77.97	17.10	31.73	23.56

Table 5. The IAEA recommended in-air criteria of neutron flux after passing through scheme A and scheme B.

Configuration	ϕ_{epi} ($\times 10^9 \text{ cm}^{-2} \text{ s}^{-1}$)	ϕ_{th} / ϕ_{epi}	D_f / ϕ_{epi} ($\times 10^{-13} \text{ Gy cm}^2$)	D_g / ϕ_{epi} ($\times 10^{-13} \text{ Gy cm}^2$)
IAEA Limits	≥ 1	~ 0.05	≤ 2	≤ 2
Scheme A	1.5	0.08	1.91	2.12
Scheme B	1.27	0.06	1.85	2.08

The epi/th represent the flux ratio of epithermal neutron to the thermal neutron.

was reduced to 66.7% of the original value (Fig. 7c). Its fast neutron dose had the greatest reduction to 25% of the original value. In addition, the photon dose decreased to 50% of the original value, and the thermal neutron dose decreased by 36.3%.

In determining the reason for the variation of dose compositions under the two schemes, neutron energy spectra in the tumor and the skin were studied. The original neutron spectrum is referred to as the neutron spectrum without the skin-shielding layer.

Compared with the original neutron spectrum, neutron flux attenuation was larger in scheme A. In the tumor, the fast neutron flux decreased, and the value of the thermal neutron flux peak was reduced to a third of the original. Thus, the fast neutron dose and boron dose to the tumor declined. Meanwhile, the proportion of boron dose increased. In the skin, the fast neutron flux declined, and the thermal neutron flux peak decreased to one-tenth of the original. This phenomenon led to the decrease in the fast and thermal neutron dose to the skin (Fig. 8a).

Compared with the decrease of the neutron flux in scheme A, that in scheme B was less. In the tumor, the attenuations of thermal and fast neutron flux were smaller than those in scheme A. Thus, the fast neutron dose and the boron dose to the tumor were higher than those in scheme A.

In the skin, the fast and thermal neutrons were weakened slightly, causing the decrease in fast neutron dose and boron dose of the skin. Moreover, the doses were higher than those in scheme A (Fig. 8b).

According to the preceding analysis, the skin dose reduction of the two skin-shielding schemes was mainly due to the reduction of the fast neutron dose. The process of fast neutron attenuated to thermal neutrons caused the fast neutron dose reduction. The material of scheme A is ⁶LiF-TP, which could slow down fast neutrons effectively because it contains hydrogen, and it reduces the skin dose apparently even with the thickness of 0.1 cm.

3.4 Influence of shielding schemes on OARs dose and second cancer risk

When the tumor achieved the prescribed dose of 32 Gy-Eq, the two shielding schemes could reduce the skin dose effectively. The maximum dose to the skin reached 42 Gy-Eq without a shielding layer. In scheme A, the skin dose decreased to 20.82 Gy-Eq, and this reduction was more obvious than that in scheme B. In scheme B, the maximum skin dose decreased to 23.57 Gy-Eq, which was also within the dose limit of 26 Gy-Eq (Fig. 9). However, the irradiation time of scheme A was 40.05 min, which was longer than that of scheme B. In comparing these two schemes for the effects of dose improvement, the OAR dose distribution needs to be further verified.

The OAR doses under the two schemes were compared. As the tumor achieved the prescribed dose of 32 Gy-Eq, the maximum dose to OARs conformed to the NCCN dose limits. For scheme A, its effect on radiation protection was good, and it reduced the OAR dose effectively. For scheme B, it could

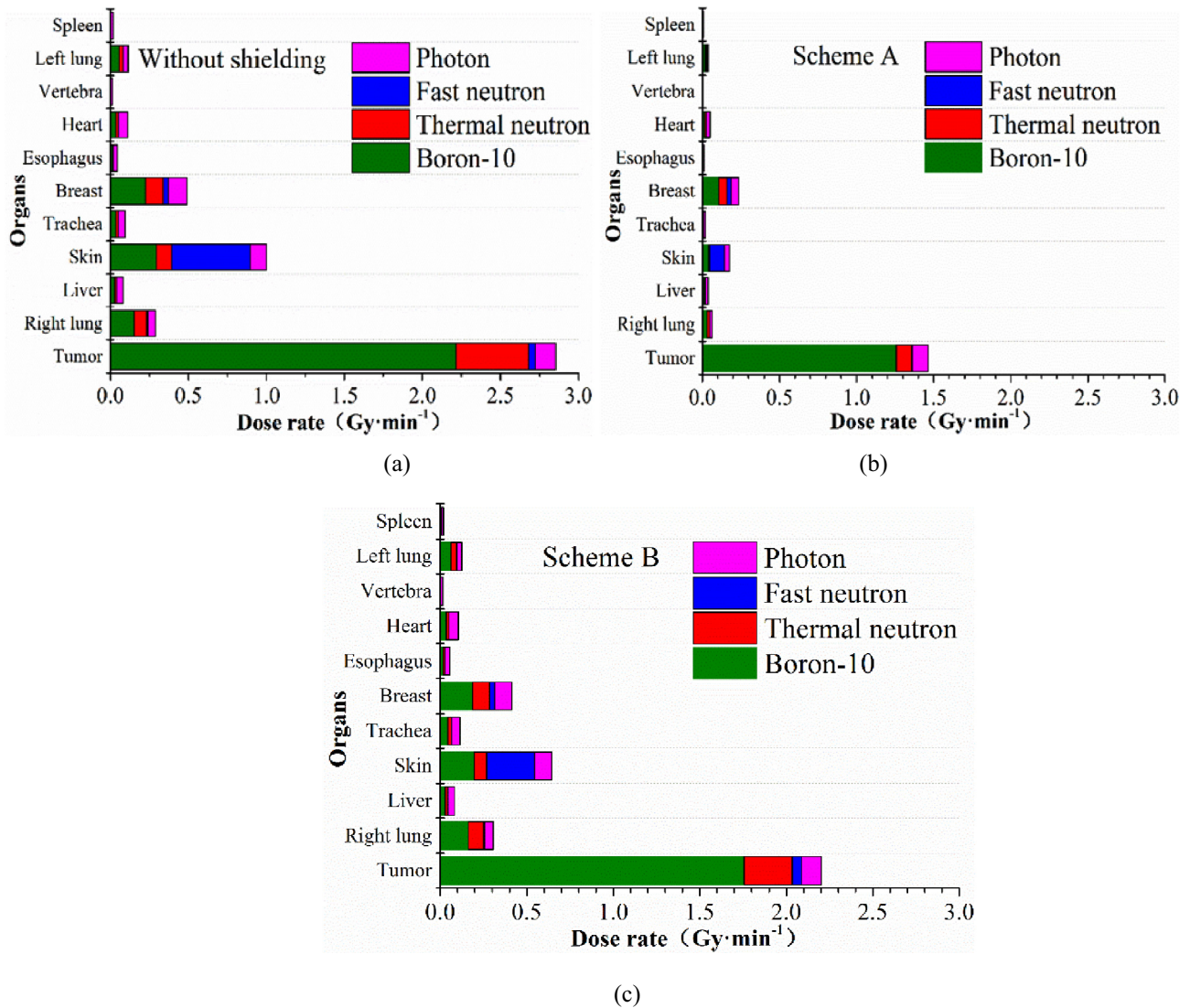


Fig. 7. Tumor and OARs dose under the different conditions: (a) without the skin-shielding layers; (b) scheme A; and (c) scheme B.

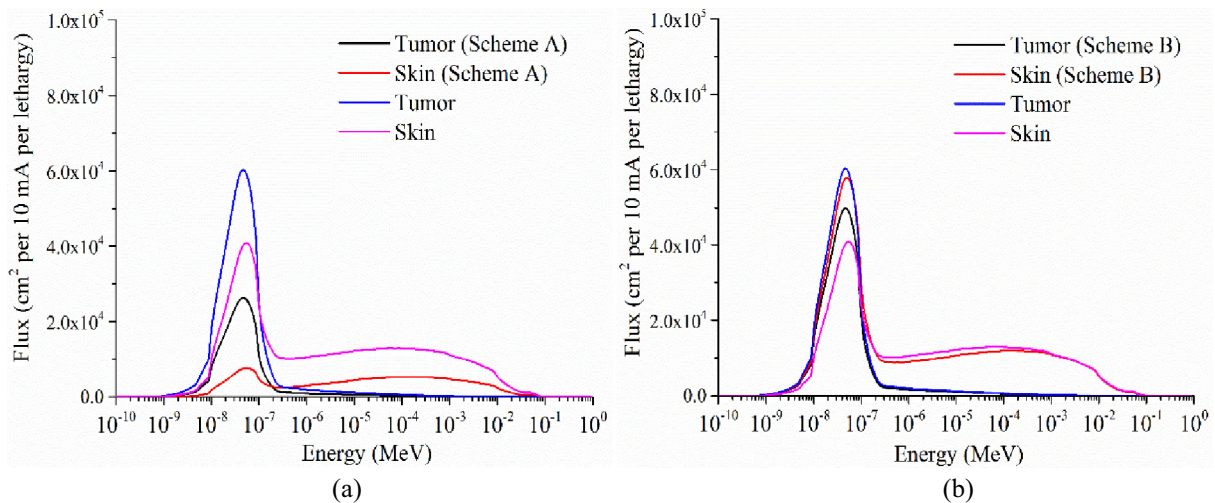


Fig. 8. Neutron spectra in the tumor and the skin: (a) scheme A and (b) scheme B.

reduce the OAR dose to a certain degree. For example, it reduced breast and trachea dose sharply. However, the dose to the left and right lungs increased under shielding by scheme B (Fig. 10).

When the tumor achieved the prescribed dose of 32 Gy-Eq, both schemes reduced the average dose to OARs to

varying degrees (Fig. 11). The risk factor was indicated in the National Council on Radiation Protection’s report number 116 (NCRP 116, 1992), and the second cancer risks were calculated to assess the two schemes. The second cancer risks of all the healthy tissues and organs were reduced by scheme A, especially the great reduction of the risk of the breast, skin, and trachea. Scheme B reduced the second cancer risks of the breast, whereas the second cancer risks of some organs, including the lung, liver, adrenal glands, and esophagus, exhibited slight increases (Tab. 6). Thus, the radiation protection effect of scheme A is better than that of scheme B.

4 Discussion

The reason for why skin dose exceed the dose limitation is that fast neutron of Neuboron source is relative large. Thus, we consider adding a skin shielding layer which could convert the fast neutron to epithermal (or thermal) neutrons. We chose the material containing ⁶Li and ¹H (Equivalent Tissue material, ⁶LiF-TP, and lithium carbonate) as the shielding layer. Because ⁶Li and ¹H have relative large cross section with neutrons (10–10⁴ keV), and they could effectively slow down the fast neutrons (>10 keV) to epithermal neutrons (0.5 eV–10 keV). For the ETM contains the most composition of H element in these three material, it moderates the most of fast neutrons to thermal neutrons.

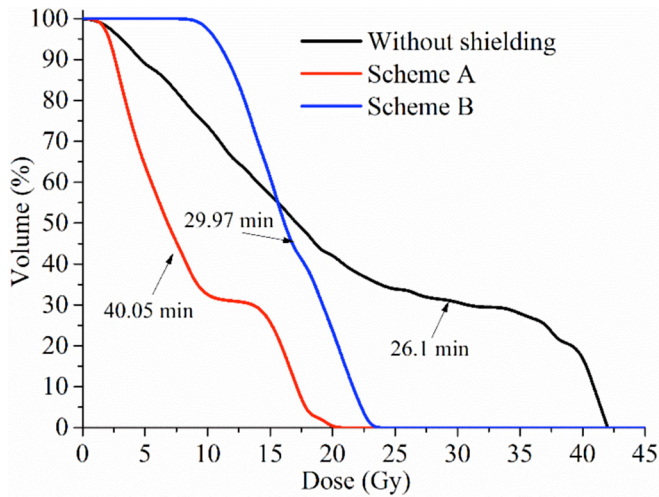


Fig. 9. Dose distribution of the skin and irradiation time under the two skin-shielding schemes.

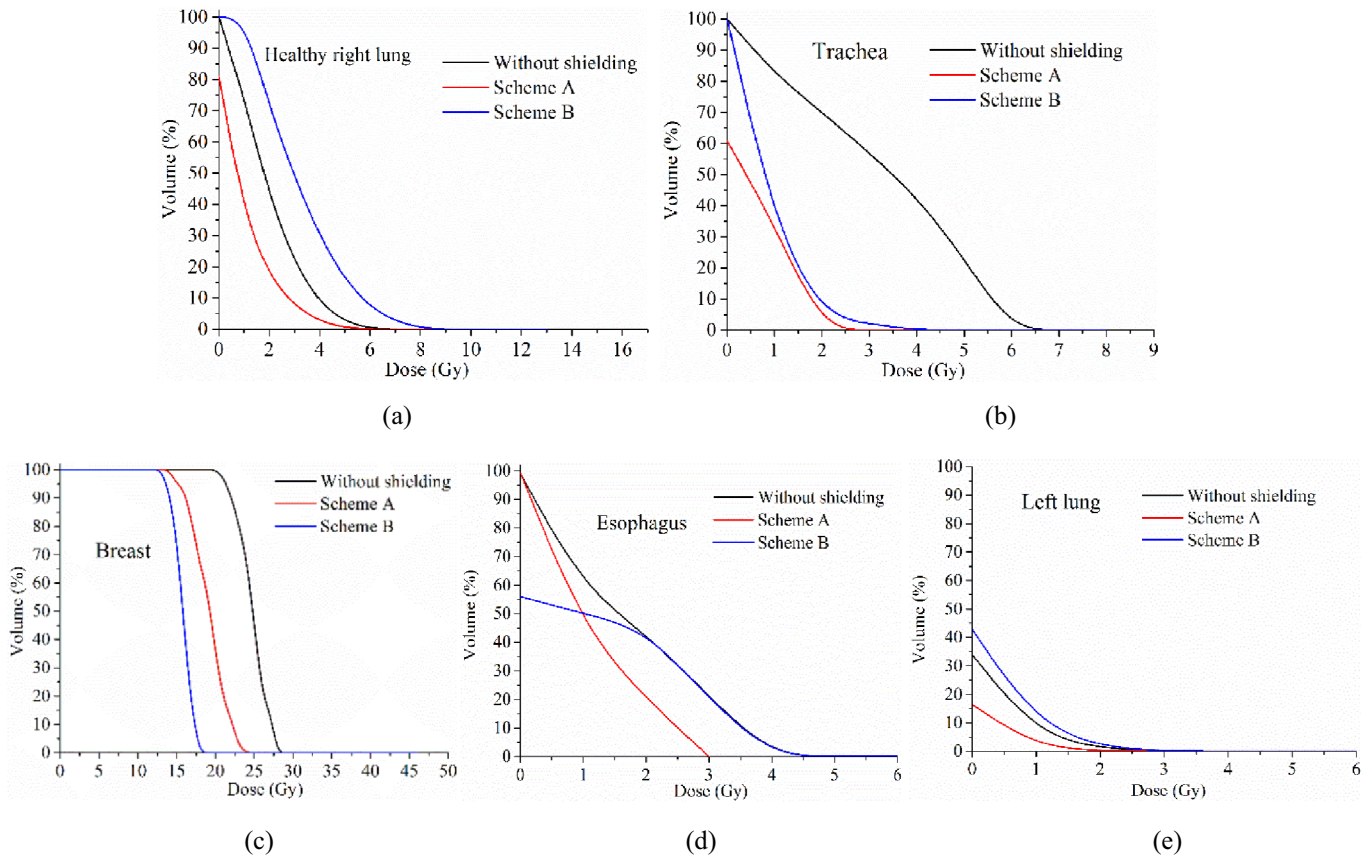
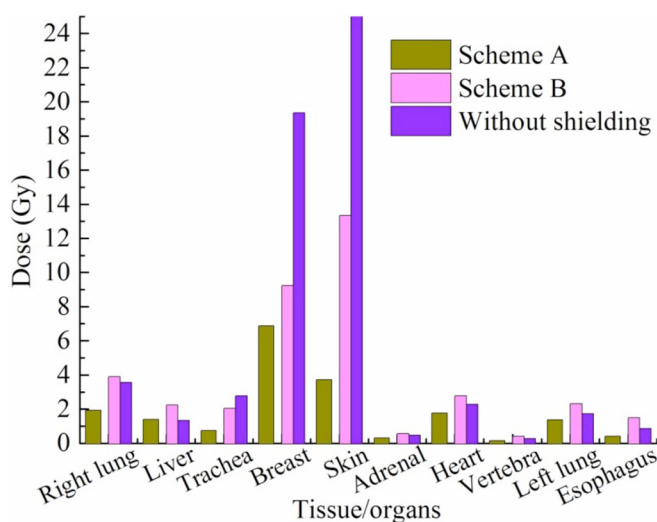


Fig. 10. Dose distribution of the OARs under the two schemes including (a) healthy right lung, (b) trachea, (c) breast, (d) esophagus, and (e) left lung.

Table 6. Second cancer risks of OARs under the two skin-shielding schemes and the condition without skin-shielding layer.

OARs	Risk factor (10^{-2} Sv^{-1})	Second cancer risk (%)		
		Without shield	Scheme A	Scheme B
Right lung	0.85	3.56	1.93	3.89
Liver	0.15	0.20	0.21	0.32
Trachea	0.50	1.29	0.37	1.12
Breast	0.20	3.87	1.37	1.79
Adrenal	0.50	0.23	0.16	0.27
Esophagus	0.30	0.26	0.12	0.43
Heart	0.50	1.14	0.89	1.34
Left lung	0.85	1.46	1.17	1.47
Skin	0.02	0.56	0.07	0.26

**Fig. 11.** Total dose to OARs under the two schemes and the condition without skin-shielding layer.

Comparing ${}^6\text{LiF-TP}$ with Li_2CO_3 , the ${}^6\text{LiF-TP}$ contains the more H element than Li_2CO_3 , thus, it reduces more epidermal neutrons than that of Li_2CO_3 , and it causes the obvious reduction of neutron flux and the longer irradiation time. Thus, Li_2CO_3 could be considered as an appropriate choice in future skin-shielding design.

There are some other approaches to reduce the skin dose, including design of adjustable beam shaping assembly, and developments of suitable neutron source and boron drug. However, currently, the method of skin-shielding design is more practical than the other approaches.

Indeed, it is worth considering that our skin-shielding design was built on an ideal irradiation condition. Certain factors, including different type of lung tumor, neutron source with different beam entry angles, and ${}^{10}\text{B}$ concentration dynamics, could affect the dose distribution in clinical application and caused diverse skin-shielding layer designs. Skin-shielding design for future practical applications should

notice as follows, first, noting that lung cancers are various (including the depth and size of tumor) is important, especially a cancer that are more centrally located lesion inside the lung. Second, actual neutron source irradiation (especially its angular distribution) should be considered. Third, the pharmacokinetic model for ${}^{10}\text{B}$ concentration is worth studying to approach the actual condition. However, although based on the ideal model, the study of skin-shielding design is also meaningful to improve the dose distribution, and it provides a feasible method for solving skin overdose problem. In the future, the skin-shielding design will be verified in clinic, however, at present, the BNCT performance in China is restricted by current medical conditions, thus, our study is theoretical based on Monte Carlo methods, it is expected to provide reference for the future BNCT performance.

5 Conclusions

The common NSCLC (depth of 7 cm) was treated with BNCT using the Neuboron source. It found that the skin dose exceeds its dose limitation. Thus, the skin-shielding layer was proposed to reduce the skin dose and improve the dose distribution of BNCT for lung cancer. The shielding layer was added between the skin surface and neutron source. Three kinds of materials (Equivalent Tissue material, ${}^6\text{LiF-TP}$, and lithium carbonate) were used as the skin-shielding layer.

According to the skin dose limit and irradiation time, two skin-shielding schemes were selected as the optimized schemes. Scheme A involved 0.1 cm-thick ${}^6\text{LiF-TP}$, and scheme B involved 0.6 cm-thick lithium carbonate. The two shielding schemes reduced the skin dose effectively but extended the irradiation time in different degrees. Compared with scheme B, scheme A had a better dose optimization effect, which reduced all OAR doses. However, it required longer irradiation time (40.05 min) than that of scheme B (29.97 min).

In this paper, scheme B reduced the skin and breast doses but increased the second cancer risk of the lungs, liver, adrenal glands, and esophagus. Fortunately, the doses to these OARs remained within the prescribed limits. For BNCT lung cancer, when the irradiation time is longer, more uncontrollable factors

will appear, causing a decline in treatment effect. For example, the offset of irradiation position (Takada *et al.*, 2016) and the change of boron concentration (Heber *et al.*, 2004) affect the dose distribution. Thus, scheme B (0.6 cm-thick lithium carbonate) was chosen as the final optimization scheme because of its short irradiation time. The method of skin-shielding design could help to meet the treatable requirement of BNCT, which could also provide a reference for other neutron sources.

Acknowledgements. This work was supported by the National Natural Science Foundation of China [Grant No. 11475087], the National Science and Technology Support Program [Grant No. 2015BAI34H00], the National Natural Science Foundation of China [Grant No. 11605117], the International Science Technology Cooperation of National Key Research and Development Program [Grant No. 2016YFE0103600], National Key Research and Development Program [Grant No. 2017YFC0107700], Foundation of Graduate Innovation Center in NUAA [Grant No. kfjj20160610], and the Priority Academic Program Development of Jiangsu Higher Education Institutions.

References

- Bayanov B, Burdakov V, Ivanov A. 2015. Readiness for boron neutron capture therap. In: *Biomedical Engineering and Computational Technologies (SIBIRCON)*, 2015, International Conference on. IEEE, pp. 27–32.
- Bortolussi S, Bakeine JG, Ballarini F. 2011. Boron uptake measurements in a rat model for Boron Neutron Capture Therapy of lung tumours. *Appl. Radiat. Isot.* 69(2): 394–398.
- Ettinger DS, Akerley W, Borghaei H. 2013. Non-small cell lung cancer, version 2. *J. Natl. Compr. Canc. Netw.* 11(6): 645–653.
- Farias RO, Bortolussi S, Menendez PR, Gonzalez SJ. 2014. Exploring Boron Neutron Capture Therapy for non-small cell lung cancer. *Phys. Medica* 30: 888–897.
- Fujimoto N *et al.*, 2015. Improvement of depth dose distribution using multiple- field irradiation in boron neutron capture therapy. *Appl. Radiat. Isot.* 106: 134–138.
- Geng CR, Tang XB, Hou XX, Shu DY, Chen D. 2014. Development of Chinese hybrid radiation adult phantoms and their application to external dosimetry. *Sci. China Technol. Sc.* 57(4): 713–719.
- Goorley JT, Kiger Lii, WS, Zamenhof RG. 2002. Reference dosimetry calculations for neutron capture therapy with comparison of analytical and voxel models. *Med. Phys.* 29(2): 145–156.
- Guitton TG, Kinaci A, Ring D. 2013. Diagnostic accuracy of 2- and 3-dimensional computed tomography and solid modeling of coronoid fractures. *J. Shoulder Elbow Surg.* 22: 782–786.
- Haiyan Y *et al.* 2017a. Impacts of multiple-field irradiation and boron concentration on the treatment of boron neutron capture therapy for non-small cell lung cancer. *Iran. J. Radiat. Res.* 15(1): 1.
- Haiyan Y *et al.* 2017b. Influence of neutron sources and ^{10}B concentration on boron neutron capture therapy for shallow and deeper non-small cell lung cancer. *Health Phys.* 112(3): 258–265.
- Heber E, Trivillin VA, Nigg D, Erica L, Kreimanna Maria E, Itoiza c, Raúl J. 2004. Biodistribution of GB-10 ($\text{Na}_2\text{B}_{10}\text{H}_{10}$) compound for boron neutron capture therapy (BNCT) in an experimental model of oral cancer in the hamster cheek pouch. *Arch. Oral Biol.* 49(4): 313–324.
- International Atomic Energy Agency. 2001. Current status of neutron capture therapy. IAEA- TECDOC-1223.
- International Commission on Radiation Units and Measurements. 1992. Photon, Electron, Proton and Neutron Interaction Data for Body Tissues. Report 46.
- International Commission on Radiological Protection. 2002. Basic anatomical and physiological data for use in radiological protection reference values. ICRP Publication 89. *Ann ICRP* 32.
- Ishiyama S. 2014. Deterministic Parsing Model of the Compound Biological Effectiveness (CBE) Factor for Intracellular ^{10}B Distribution in Boron Neutron Capture Therapy. *J. Cancer Ther.* 5 (14): 1388.
- Kiger JL. 2006. Radiobiology of normal rat lung in boron neutron capture therapy. Cambridge, Massachusetts, USA: Massachusetts Institute of Technology.
- Krstic D, Markovic VM, Jovanovic Z, Milenkovic B, Nikezic D, Atanackovic J. 2014. Monte Carlo calculations of lung dose in ORNL phantom for boron neutron capture therapy. *Radiat. Prot. Dosim.* 161: 269–273.
- Lee PY *et al.* 2014. Dosimetric performance evaluation regarding proton beam incident angles of a lithium-based AB-BNCT design. *Radiat. Prot. Dosim.* 161: 403–409.
- Liu YWH, Chang CT, Yeh LY, Wang LW, Lin TY. 2013. BNCT treatment planning for superficial and deep-seated tumors: Experience from clinical trial of recurrent head and neck cancer at THOR. *Appl. Radiat. Isot.* 106: 121–124.
- National Council on Radiation Protection and Measurements. 1992. Limitation of exposure to ionizing radiation NCRP Report No. 116.
- Norbash AM, Busick D, Marks MP. 1996. Techniques for reducing interventional neuroradiologic skin dose: tube position rotation and supplemental beam filtration. *Am. J. Neuroradiol.* 17: 41–49.
- Ryynanen PM, Kortensniemi M. 2000. Models for estimation of the ^{10}B concentration after BPA-fructose complex infusion in patients during epithermal neutron irradiation in BNCT International. *Int. J. Radiat. Oncol.* 48: 1145–1154.
- Sakurai Y, Ono K. 2007. Improvement of dose distribution by central beam shielding in boron neutron capture therapy. *Phys. Med. Biol.* 52(24): 7409.
- Sutlief SG. 2015. Protection and measurement in radiation therapy. *Health Phys.* 108(2): 224–241.
- Suzuki M, Suzuki O, Sakurai Y. 2012. Reirradiation for locally recurrent lung cancer in the chest wall with boron neutron capture therapy (BNCT). *Int. Cancer Conf. J. Springer Japan* 1(4): 235–238.
- Takada K, Kumada H, Liem PH. 2016. Development of Monte Carlo based real-time treatment planning system with fast calculation algorithm for boron neutron capture therapy. *Physica Medica: Eur. J. Med. Phys.* 32(12): 1846–1851.
- Trivillin VA, Heber EM, Itoiz ME. 2004. Radiobiology of bnc mediated by GB-10 and GB-10+BPA in experimental oral cancer. *Appl. Radiat. Isot.* 61: 939–945.